Journal of Power Sources 205 (2012) 57–62

Contents lists available at SciVerse ScienceDirect

Journal of Power Sources

journal homepage: www.elsevier.com/locate/jpowsour

Feasibility and mechanism of lithium oxide as sintering aid for $Ce_{0.8}Sm_{0.2}O_{\delta}$ electrolyte

Shuai Li, Cunni Xian, Kai Yang, Chunwen Sun, Zhaoxiang Wang*, Liquan Chen

Renewable Energy Laboratory, Institute of Physics, Chinese Academy of Sciences, P.O. Box 603, Beijing 100190, China

ARTICLE INFO

Article history:
Received 20 September 2011
Received in revised form
13 December 2011
Accepted 1 January 2012
Available online 9 January 2012

Keywords:
Sintering aid
Lithium oxide
Liquid sintering mechanism
Solid oxide fuel cell

ABSTRACT

Cerium oxide is a promising material for electrodes and electrolytes of solid oxide fuel cells (SOFCs). Lowering the sintering temperature of the electrolyte will bring a lot of benefits to the fabrication of SOFCs. This paper evaluates the feasibility of using lithium oxide as a sintering aid to reduce the densification temperature of samarium-doped ceria ($Ce_{0.8}Sm_{0.2}O_{1.9}$, SDC) by SEM and electrochemical impedance spectroscopy. It is shown that the addition of Li_2CO_3 can indeed decrease the sintering temperature of SDC. More attention is paid to understand the aiding mechanism of Li_2CO_3. Raman spectroscopy and thermal analysis indicate that it is Li_2O, a decomposition product of Li_2CO_3, that facilitates the sintering by way of a liquid phase sintering effect on the grain boundaries of SDC. These findings help to promote the application of ceria-based electrolytes for intermediate temperature SOFCs.

1. Introduction

Solid oxide fuel cells (SOFCs) convert the chemical energy of the fuels directly into electrical energy with high efficiency [1–4]. Intermediate temperature SOFC has drawn much attention due to its lower operation temperature [5]. Cerium oxide (ceria) has been widely studied as SOFC electrode materials because they exhibit high mixed conductivity in both reductive and oxidative atmospheres, high catalytic activity for the oxygen reduction on the cathode and reforming capability to the hydrocarbons on the anode [6–9]. At lower temperatures, doped ceria electrolyte materials are superior to the yttria stabilized zirconia (YSZ) in ionic conductivity [1,5,10]. 20 mol% samarium-doped ceria (SDC) was reported to have ionic conductivities up to 1.5×10^{-2} S cm^{-1} at 700 °C [10,11]. However, CeO_2-based materials are known hard to be densify below 1200 °C [12]. Increasing the sintering temperature will induce a series of problems such as grain growth and interfacial reactions between electrolyte and electrodes, harmful to the cell manufacture and its electrochemical performances.

Two ways have been proposed to lower the sintering temperature. One is to reduce the particle size to enhance the activity of the material [13], the other is to use some additives such as Cu, Co, Fe, Mn, Li and Zn as sintering aids [14,15]. The second method can effectively reduce the sintering temperature while ensure the densification of the material. Various mechanisms have been proposed to explain the eased sintering, such as beneficial liquid formation, dopant substitution, and dopant segregations on the grain boundaries [14–16]. Liu et al. [17] increased the conductivity of gadolinium-doped ceria by the addition of Li or Co. In other successful cases, Gauckler et al. [18,19] attributed the enhanced conductivity to the electronic conduction due to segregation or dissolution of heavy metal oxides on the grain boundaries. Similarly, Esposito et al. [16] believed that the added salt $LiNO_3$ melts and evaporates in large part during sintering, and thus, enhances the ionic conductivity especially at the grain boundaries. However, the aiding mechanism is still not clear yet.

Considering that Li has the highest saturation vapor pressure of the above aiding elements, we employ Li_2CO_3 as a sintering aid in this work. We will evaluate the feasibility of using Li_2O as a sintering aid and its impacts on the conductivity of $Ce_{0.8}Sm_{0.2}O_{1.9}$. Based on extended physical characterizations, the sintering mechanism is better understood.

2. Experimental

Commercial hydrate cerium (III) nitrate (AR, 99%), hydrate samarium nitrate (AR, 99%), citric acid and lithium carbonate were mixed and dissolved in de-ionized water at a molar ratio of 1:4 for Sm^{3+}:Ce^{3+} and 3:2 for the citric acid to the metallic ions (Sm^{3+} and Ce^{3+}). The molar fractions of Li^+ were 0, 3%, 5%, 10% and 15%, respectively. The solution was continuously stirred at 90 °C until a dry precursor was obtained. Combustion occurred as the dry mixture was further heated. The combustion product was calcinated at 700 °C for 10 h in air. The as-prepared powder (or their pellet) was

* Corresponding author. Tel.: +86 10 82649050; fax: +86 10 82649050.
E-mail address: zxwang@iphy.ac.cn (Z. Wang).

0378-7753/$ – see front matter © 2012 Elsevier B.V. All rights reserved.
doi:10.1016/j.jpowsour.2012.01.010

referred to as SDC, SDC-Li-3, SDC-Li-5, SDC-Li-10 and SDC-Li-15, respectively, depending on the Li content in each.

The powder was mixed with polyvinylbutyral binder, pressed into Ø15 mm × 1 mm pellet and sintered between 900 and 1400 °C for 10 h under different atmospheres. After cooled down naturally, conducting silver paste was brushed uniformly on the pellet and then heated at 750 °C for 0.5 h before the electrochemical impedance spectroscopic (EIS) measurement was carried out on an IM6e electrochemical station in air (50 mV perturbation voltage and the frequency between 3 MHz and 100 mHz).

The microstructure of the sintered pellet was characterized on a Holland X'Pert Pro MPD X-ray diffractometer equipped with a monochromatized Cu *K*α radiation and a JY HR800 Raman spectrometer at room temperature. The incident laser was 514.5 nm and the resolution of the Raman spectrometer was set to 2 cm^{-1}. The morphology of the cross section of the sintered pellet was observed on an XL30s-FEG scanning electron microscope (accelerating voltage 10 kV). The chemical composition of the sintered pellets was analyzed by the inductively coupled plasma method (ICP, Thermo Electron Corporation). The thermogravimetry (TG) and differential scanning calorimetry (DSC) were carried out on Netsch STA 449C. The mass flow spectrometry (Netsch 403C Aeolos II quadrupole) was recorded synchronously with the TG–DSC information.

3. Results and discussion

It is reported that thermal decomposition of pure Li_2CO_3 begins at its melting point of 720 °C [20]. Our DSC and CO_2 mass flow spectrum (Fig. 1a) show that the thermal decomposition of Li_2CO_3 takes place at *ca.* 710 °C and reaches its summit at 900 °C in argon when it is mixed with SDC. The Li_2CO_3-containing SDC pellet becomes densified at 1000 °C in argon (Fig. 1b) and air (Fig. 1c).

Fig. 2 compares the morphology of the SDC before and after Li_2CO_3 is added and sintered at different temperatures in air. A lot of large holes can be observed in the Li_2CO_3-free SDC pellet until 1400 °C. However, when 5 mol% and 10 mol% Li are added, the SDC pellets become densified at 1000 °C and 900 °C, respectively. It is obvious that Li_2CO_3 is an effective sintering aid of the SDC.

In order to evaluate the influence of the sintering aid on the electrical properties of the SDC, the EI spectra of the Li_2CO_3-added and the Li_2CO_3-free SDC pellets were recorded (Fig. 3). It is seen that the shape of the EIS of the same SDC pellets is closely related to the measurement temperature. Therefore, different equivalent circuits have to be employed to fit the EIS spectra in different temperature ranges. The EI spectrum is composed of two well-defined semicircles and one slope at low temperature (300–400 °C; Fig. 3a). The high- and low-frequency semicircles are attributed to the bulk and the grain boundary impedances, respectively. As the temperature increases (400–600 °C) (Fig. 3b), the semi-circle for the bulk impedance disappears. The high- and low-frequency semicircles are for the grain boundary and electrode polarization impedances, respectively. When the temperature is above 600 °C (Fig. 3c), the low-frequency semicircle becomes a large arc. The electrode polarization impedance becomes dominant while the grain boundary impedance is too small to fit.

Fig. 4 summarizes the fitting results to the EI spectra. The temperature-dependent bulk and grain boundary conductivities of the SDC with or without Li_2CO_3 obey the Arrhenius equation in all the studied temperature range. For the Li_2CO_3-free SDC, the bulk, the grain boundary and the total conductivities at 474 °C are 0.0136, 0.0116 and 0.0063 S cm^{-1}, respectively, while their activation energies are fitted to be 1.135, 1.416 and 1.617 eV, respectively.

Fig. 4 also indicates that the addition of Li_2CO_3 has greater influence on the grain boundary conductivity of SDC than on its bulk conductivity. The bulk conductivity of the SDC does not depend

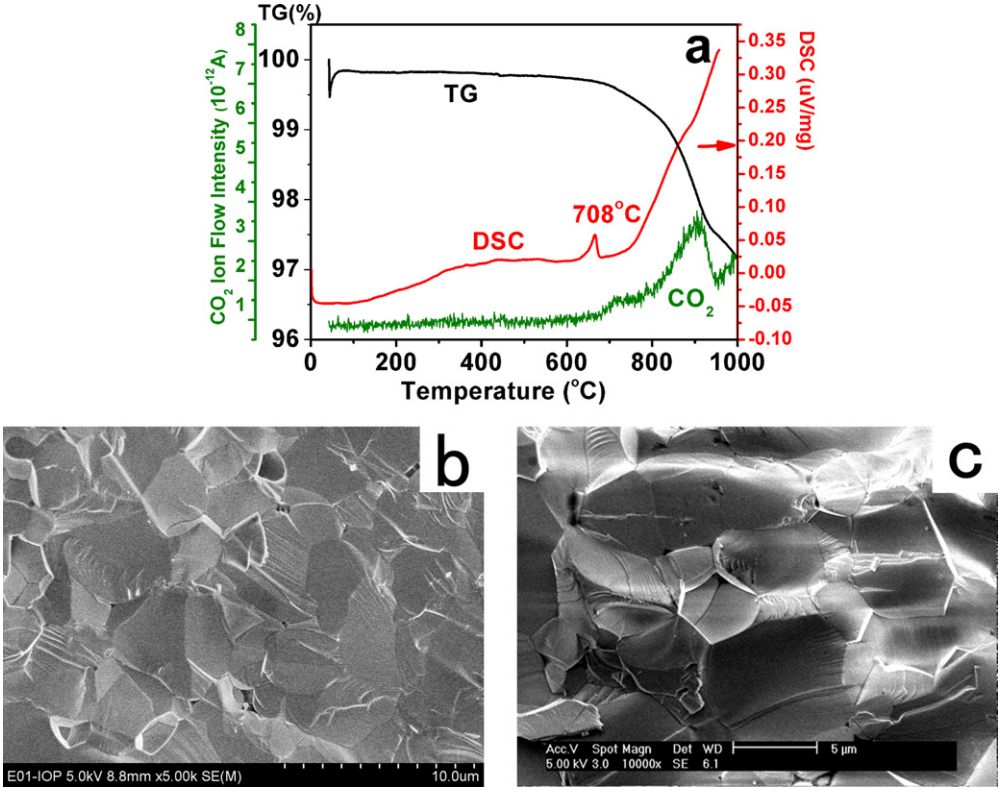

Fig. 1. The thermal analysis (differential scanning calorimetry, thermogravimetry and the CO_2 mass flow spectrum) of the SDC-Li-15 sample in Ar (a), the morphology of the cross sections of SDC-Li-15 after sintered at 1000 °C in Ar for 10 h (b), and at 1000 °C in air for 10 h (c).

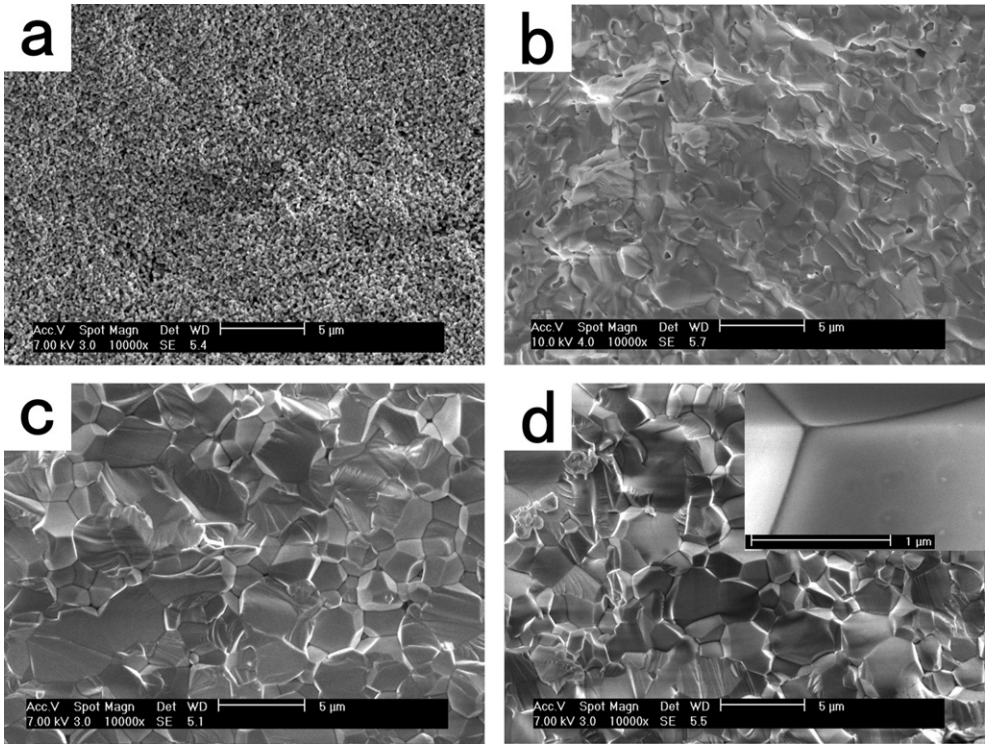

Fig. 2. Comparison of the cross sections of Li_2CO_3-free SDC sintered in air at 800 °C (a) and at 1400 °C (b), and the SDC-Li-5 sintered in air at 1000 °C (c) and SCD-Li-10 sintered at 900 °C (d) for 10 h.

either on the content of the added Li_2CO_3 or on the sintering temperature (Fig. 4a and c). On one hand, the grain boundary conductivities of the Li_2CO_3-added SDC sintered at 1000 °C for 10 h are all slightly lower than that of the Li_2CO_3-free SDC (Fig. 4b). However, it seems that the content of the added Li_2CO_3 has even less impact on the grain boundary conductivity as long as the SDC can be densified at 1000 °C; the difference of the grain boundary conductivity of the SDC containing 5%, 10% and 15% Li_2CO_3 is very

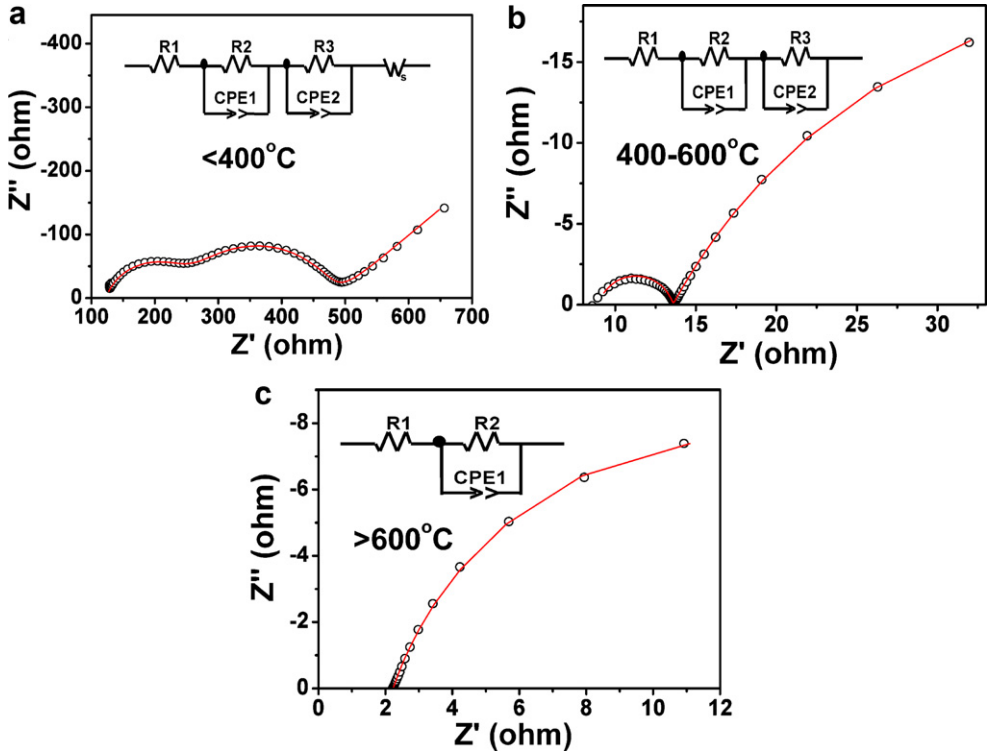

Fig. 3. The typical EI spectra and the equivalent circuits of the sintered SDC (independent of sintering temperature, atmosphere and the content of Li_2CO_3) in different measurement temperatures ranges.

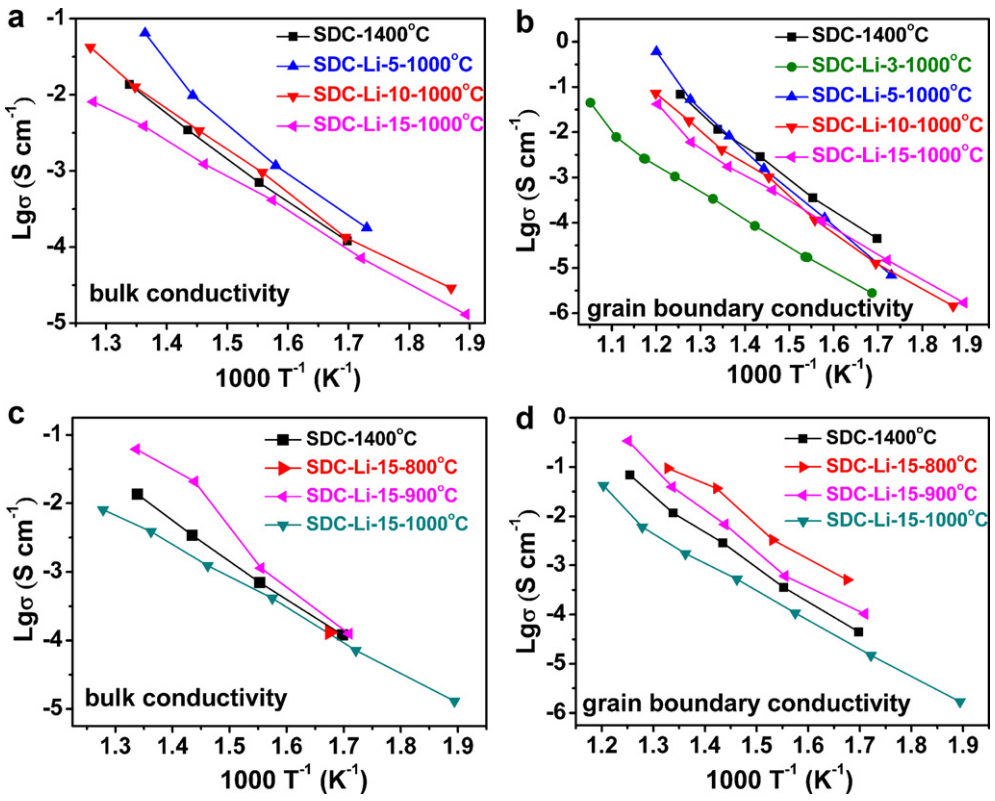

Fig. 4. The Arrhenius plots of the bulk (a and c) and the grain boundary (b and d) conductivities of the SDC containing different contents of Li_2CO_3 and sintered at different temperatures in air.

subtle in (Fig. 4b). On the other hand, the grain boundary conductivity of the Li_2CO_3-added SDC (*e.g.* SDC-Li-15) increases as the sintering temperature decreases from 1000 °C to 800 °C. The grain boundary conductivity of the low-temperature-sintered SDC-Li-15 is even higher than that of the Li_2CO_3-free SDC (Fig. 4d).

There have been arguments on how the sintering aid influences the structure and the conductivity of the SDC host. Gourishankar et al. [21] reported that lithium reacts with CeO_2 to form new compounds such as $LiCeO_2$ and Li_3CeO_3. Xia et al. [22] attributed the increased conductivity to the ions such as Li^+, O^{2-} and CO_3^{2-} that transport *via* the consecutive interfaces. Liu et al. [17] found that the addition of a sintering aid helps to increase the conductivity of the electrolyte without lowering the open-circuit voltage of the cell. However, our XRD (sensitive to the crystallites; Fig. 5A) and

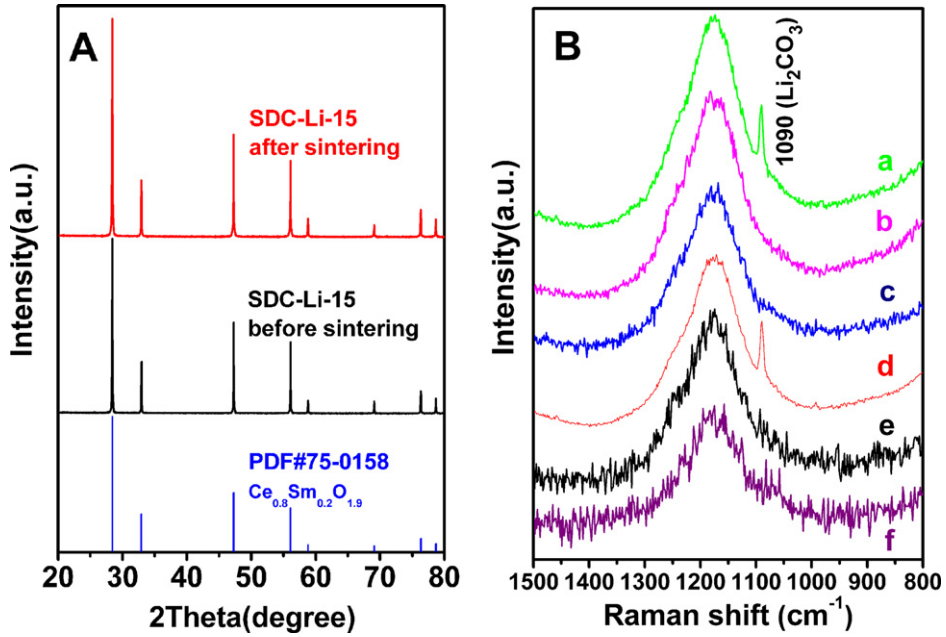

Fig. 5. The XRD patterns (A) of SDC-Li-15 sintered at 1000 °C for 10 h and the Raman spectra (B; non-sintered SDC-Li-15 (a), SDC-Li-15 sintered for 10 h in CO_2 and then 10 h in air (b), 10 h in air and then 10 h in CO_2 (c), 10 h in CO_2 (d), 10 h in air (e), and pure SDC (f).

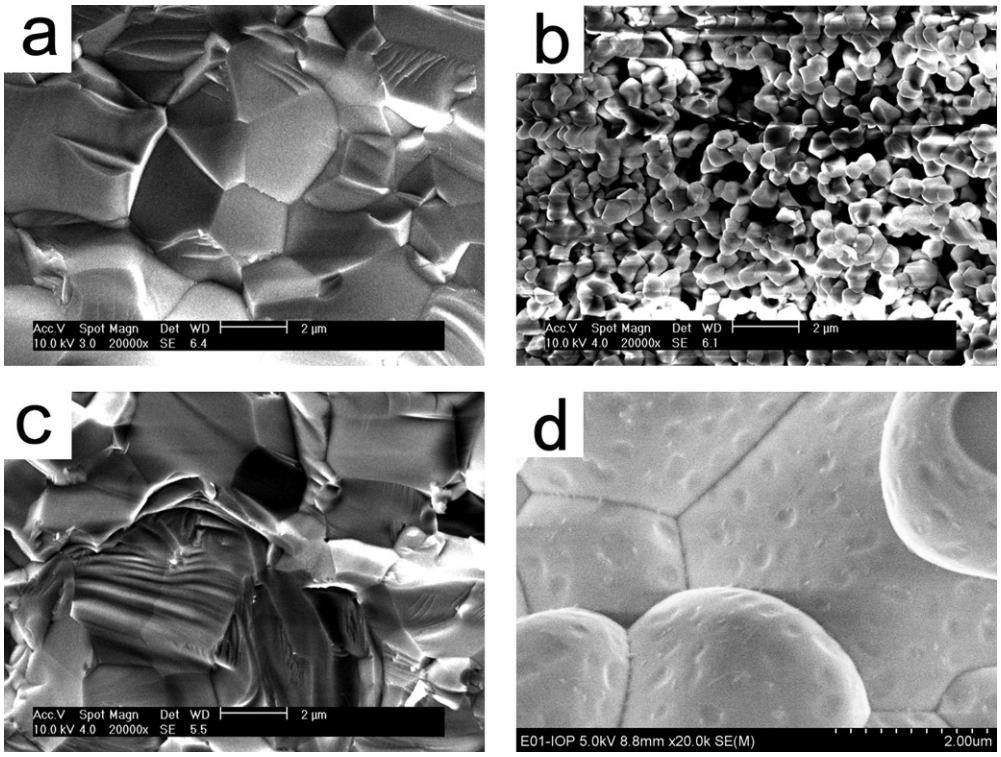

Fig. 6. Comparison of the morphology of SDC-Li-15 sintered at 1000 °C for 10 h in air (a), in CO_2 (b), 10 h in CO_2 and then more 10 h in air (c), and in Ar (d).

Raman spectroscopic (sensitive to both the amorphous and well-crystallized materials; Fig. 5B) studies indicate that adding Li_2CO_3 in SDC does not produce any new phases or induce any detectable structural changes in SDC. This makes it easy to understand why addition of the sintering aid does not change the bulk conductivity of the SDC. Our ICP analysis shows that no trace of lithium can be detected in the SDC-Li-15 ceramics sintered at 1000 °C for 10 h in air, but 1.5 mol% of Li is left in the 800 °C-sintered SDC-Li-15. This might imply that the lithium contributes to increase the grain boundary conductivity of the SDC. At higher sintering temperatures, the lithium disappears and the SDC particles grow bigger, both resulting in lower grain boundary conductivity. These findings are confirmed by the following analysis. Of course, addition of 3 mol% Li decreases the grain boundary conductivity of SDC by more than one magnitude (Fig. 4b) because such SDC pellet cannot be densified up to 1000 °C.

In order to understand how the added Li_2CO_3 facilitates the sintering of the SDC, Fig. 6 compares the morphology of the SDC-Li-15 sintered under different atmospheres. It shows that the pellets sintered in air can be densified at 1000 °C but those sintered in CO_2 cannot. As the added Li_2CO_3 cannot be decomposed in CO_2 but disappears after sintered at 1000 °C in air (Fig. 5B), these indicate that the decomposition of Li_2CO_3 is essential for the densification of SDC at lowered temperature. Considering the CO_2 mass flow spectrum (Fig. 1a), we believe that the presence of Li_2O is essential for the densification of the SDC at lowered temperatures. On the other hand, XRD and Raman characterizations show that no new phases neither crystalline nor amorphous, or structural parameter variations can be observed on sintering the SDC-Li-15 pellet. Based on the Raman, XRD, SEM, thermal and ICP analyses, it is easy to understand what facilitates the sintering of SDC is Li_2O, the decomposition product of Li_2CO_3, rather than Li_2CO_3 itself. Without the decomposition of Li_2CO_3, the densification temperature of SDC cannot be decreased.

As is shown in Fig. 6d and the inset of Fig. 2d, there are small particles and pits close to the grain boundaries of the Li_2CO_3-added SDC sintered in Ar and air, respectively. However, no such pits are observed in the sintered Li_2CO_3-free SDC pellet. Correlating these observations with the results of thermal analysis and the Raman spectroscopy, we believe that the Li_2O melts and wets the neighboring SDC grains at high temperatures and welts them together. With the sintering time increasing, the Li_2O evaporates and becomes undetectable. This is a typical process of liquid phase sintering.

Based on the above results, addition of Li_2CO_3 in SDC decreases the densification temperature of SDC. The added Li does not enter the lattice of the SDC powder or the sintered SDC. Nor does the addition of Li_2CO_3 create any new compounds. Therefore, using Li_2CO_3 as a sintering aid does not change the electrical conductivity of the bulk of SDC. However, addition of Li_2CO_3 increases the electrical conductivity of the grain boundaries of low-temperature (800 °C, for example) sintered SDC, probably due to migration of Li^+ ions and the collective effect of the melted Li_2O to the impurities on the SDC grain boundaries. At higher sintering temperatures, nevertheless, the grain boundary conductivity decreases with increasing sintering temperature. This is understandable because the SDC particles grow bigger and the Li_2O is evaporated at high temperatures.

4. Conclusions

Li_2CO_3, or to be exact, its decomposition product, Li_2O, is an effective sintering aid in lowering the densification temperature of samarium-doped ceria (SDC). Addition of Li_2CO_3 does not change the bulk conductivity of SDC because Li does not enter the lattice of SDC or participate in the formation of new compounds. At lower sintering temperatures, the grain boundary conductivity is increased by the Li^+ migration and the collective effect of the melted Li_2O on the impurities on the SDC grain boundaries. At higher sintering temperatures, however, the Li_2O evaporates and the SDC particles grow bigger, both resulting in lower grain boundary conductivity. We clarify that the Li_2O facilitates the sintering by way of a liquid phase sintering mechanism. These findings help to

understand the sintering mechanism and to promote the application of ceria-based electrolytes for SOFCs.

Acknowledgments

The authors are grateful for the financial support by the NSFC Key Project (Grant No. 50730004), the National 973 Project (Grant No. 2012CB215402) and the NSFC Project (Grant No. 51172275) of China.

References

[1] B.C.H. Steele, A. Heinzel, Nature 414 (2001) 345–352.
[2] N.Q. Minh, Solid State Ionics 174 (2004) 271–277.
[3] R.M. Ormerod, Chem. Soc. Rev. 32 (2003) 17–28.
[4] S.C. Singhal, Solid State Ionics 152–153 (2002) 405–410.
[5] D.J.L. Brett, A. Atkinson, N.P. Brandon, S.J. Skinner, Chem. Soc. Rev. 37 (2008) 1568–1578.
[6] C.W. Sun, U. Stimming, J. Power Sources 171 (2007) 247–260.
[7] C. Gaidillere, P. Vernoux, C. Mirodatos, G. Caboche, D. Farrusseng, Catal. Today 157 (2010) 263–269.
[8] D. Perez-Coll, D. Marrero-Lopez, J.C. Ruiz-Morales, P. Nunez, J.C.C. Avrantes, J.R. Frade, J. Power Sources 173 (2007) 291–297.
[9] N. Takashi, K. Tsuneyuki, Y. Keiji, K. Atsushi, O. Takanori, S. Kazuhisa, M. Junichiro, K. Tatsuya, J. Electrochem. Soc. 155 (2008) B563–B569.
[10] H. Inaba, H. Tagawa, Solid State Ionics 83 (1996) 1–16.
[11] V.V. Khartona, F.M.B. Marquesa, A. Atkinson, Solid State Ionics 174 (2004) 135–149.
[12] Y.C. Zhou, M.N. Rahaman, J. Mater. Res. 8 (1993) 1680–1686.
[13] C. Herring, J. Appl. Phys. 21 (1950) 301–303.
[14] J.D. Nicholas, L.C.D. Jonghe, Solid State Ionics 178 (2007) 1187–1194.
[15] C. Kleinlogel, L.J. Gauckler, Adv. Mater. 13 (2001) 1081–1085.
[16] V. Esposito, M. Zunic, E. Traversa, Solid State Ionics 180 (2009) 1069–1075.
[17] Z. Liu, Z. Lei, S.D. Song, L. Yu, M.F. Han, Prog. Chem. 23 (2011) 470–476.
[18] Z.L. Zhang, W. Sigle, M. Rühle, E. Jud, L.J. Gauckler, Acta Mater. 55 (2007) 2907.
[19] E. Jud, L. Gauckler, S. Halim, W. Stark, J. Am. Ceram. Soc. 89 (2006) 2970.
[20] J.W. Kim, H.G. Lee, Metall. Mater. Trans. B 32B (2001) 17–24.
[21] K.V. Gourishankar, G.K. Johnson, I. Johnson, Metall. Mater. Trans. B 28B (1997) 1103–1110.
[22] C. Xia, Y. Li, Y. Tian, Q.H. Liu, Z.M. Wang, L.J. Jia, Y.C. Zhao, Y.D. Li, J. Power Sources 195 (2010) 3149–3315.